

Soliton-limited Superflow in $^3\text{He-A}$ between Parallel Plates

J. Kopu and E. V. Thuneberg

Low Temperature Laboratory, Helsinki University of Technology, Finland

We have studied theoretically the flow of superfluid $^3\text{He-A}$ in parallel-plate geometry. The equilibrium order-parameter texture is calculated numerically in two spatial dimensions consisting of the coordinates along the flow direction and perpendicular to the plates. The calculations have been done using the hydrostatic theory in the Ginzburg-Landau region and assuming a large external magnetic field perpendicular to the plane of calculation. We have studied a uniform texture and a dipole-unlocked splay soliton as initial configurations. In the former case we find the Fredericksz transition and a helical instability with increasing flow. In the latter case we find instability in the soliton. This instability is closely related to the critical velocity in the presence of a vortex sheet. Also, the transverse NMR frequency shift at the soliton has been calculated.

PACS numbers: 67.57.Fg

1. Introduction

The anisotropic A phase of superfluid ^3He exhibits unique behavior under externally applied superflow. Instead of being quantized, the circulation of the superfluid velocity \mathbf{v}_s in $^3\text{He-A}$ can have any value depending on the spatial variation of the order-parameter texture. The decay of superflow can be accomplished by generating a nonuniform texture of the orbital vector $\hat{\mathbf{l}}$, leading ultimately to the formation of continuous vortices (with no singular core). However, energy considerations favor the uniform texture with constant $\hat{\mathbf{l}}$ for small velocities and postpone these processes until a certain critical velocity is exceeded. Because of the macroscopic length scale of texture variations and the boundary condition that fixes the direction of $\hat{\mathbf{l}}$ at the walls, vortex formation is unaffected by extrinsic influences, such as surface roughness and thermal and quantum fluctuations. Therefore, in contrast

to superfluid ^4He , critical velocity in $^3\text{He-A}$ is determined by an intrinsic instability of the flow.

Superflow of $^3\text{He-A}$ has been previously studied theoretically in many papers, see Refs. 1 and 2 for references. Essentially all of them consider only one-dimensional flow. Here we present the first truly two-dimensional calculation for $^3\text{He-A}$ in the presence of external flow. We study a flow channel consisting of parallel plates. With increasing flow, an initially constant texture becomes first modified in the Fredericksz transition, where $\hat{\mathbf{l}}$ starts to tilt from the direction normal to the plates^{3,4}. On increasing the velocity further, the texture becomes unstable towards a helical deformation^{5,6}, which leads to formation of vortices. However, the main point in this paper is to study an initially inhomogeneous texture formed by a dipole-unlocked soliton⁷. The flow through such a domain wall was first studied by Vollhardt and Maki⁸ using a variational ansatz. More recently the same problem was studied numerically in Ref. 2. We extend these one-dimensional calculations to include the effect of lateral walls in a flow channel. We investigate how the critical velocity in the presence of the soliton depends on the width D of the flow channel. We find that the dependence is much stronger than for the helical instability in the absence of the soliton.

The dipole-locked soliton is exceptionally interesting, because it forms the backbone of another topological object, the vortex sheet⁹. Our calculation can be used as a model for the critical velocity of the sheet, and it explains semi-quantitatively the measured dependence on the angular velocity¹⁰. Peculiar dynamical properties of the vortex sheet was observed in experiments¹¹. To provide additional information to explain this behavior, we have also calculated numerically the NMR frequency shift which is the relevant experimental parameter. The shifts are determined as functions of flow velocity and the separation between the plates.

2. Hydrostatic theory

Our starting point is very similar to that in Ref. 2. Here we repeat the main points. The A-phase order parameter $\overset{\leftrightarrow}{A}$ is a 3×3 tensor defined by two orthogonal unit vectors $\hat{\mathbf{m}}$ and $\hat{\mathbf{n}}$ in the orbital space and a unit vector $\hat{\mathbf{d}}$ in the spin space and has the form¹ (with real Δ)

$$A_{\mu j} = \Delta \hat{d}_\mu (\hat{m}_j + i \hat{n}_j). \quad (1)$$

One defines $\hat{\mathbf{l}} \equiv \hat{\mathbf{m}} \times \hat{\mathbf{n}}$ and a superfluid velocity as

$$\mathbf{v}_s = \frac{\hbar}{2m_3} \sum_j \hat{m}_j \nabla \hat{n}_j, \quad (2)$$

Soliton-limited superflow in $^3\text{He-A}$ between parallel plates

where m_3 is the mass of a ^3He atom. The equilibrium form of the order-parameter texture corresponds to a minimum of the hydrostatic free energy. In order to avoid dealing with complicated constraints between $\hat{\mathbf{I}}$ and \mathbf{v}_s , we express the free energy in terms of the unit-vector fields $\hat{\mathbf{m}}(\mathbf{r})$, $\hat{\mathbf{n}}(\mathbf{r})$, and $\hat{\mathbf{d}}(\mathbf{r})$. For simplicity, we restrict all our calculations to the Ginzburg-Landau region ($T_c - T \ll T_c$). The energy density consists of the dipole-dipole energy

$$f_d = \frac{1}{2}\lambda_d \left[(\hat{\mathbf{d}} \cdot \hat{\mathbf{m}})^2 + (\hat{\mathbf{d}} \cdot \hat{\mathbf{n}})^2 \right], \quad (3)$$

the magnetic-field energy

$$f_h = \frac{1}{2}\lambda_h (\hat{\mathbf{d}} \cdot \mathbf{H})^2, \quad (4)$$

and the gradient energy

$$f_g = \frac{\hbar^2 \rho_{\parallel}}{16m_3^2} \left\{ \sum_{ik} \left[(\nabla_i \hat{m}_k)^2 + (\nabla_i \hat{n}_k)^2 \right] + (\gamma - 1) (\nabla \cdot \hat{\mathbf{m}})^2 \right. \\ \left. + (\nabla \cdot \hat{\mathbf{n}})^2 + \sum_i (\hat{\mathbf{m}} \cdot \nabla \hat{d}_i)^2 + \sum_i (\hat{\mathbf{n}} \cdot \nabla \hat{d}_i)^2 \right\} + 2 \sum_{ik} (\nabla_i \hat{d}_k)^2, \quad (5)$$

see Ref. 12 for details. Generally, the superfluid density is anisotropic with components ρ_{\parallel} and ρ_{\perp} corresponding to the flow parallel and perpendicular to $\hat{\mathbf{I}}$, respectively. In the Ginzburg-Landau region with the weak-coupling value $\gamma = 3$, they differ by a factor of two: $\rho_{\perp} = 2\rho_{\parallel}$. The supercurrent density is given by

$$j_{s,k} = \frac{\hbar \rho_{\parallel}}{4m_3} \sum_j \left[(\gamma - 2) (\hat{m}_k \nabla_j \hat{n}_j - \hat{n}_k \nabla_j \hat{m}_j) \right. \\ \left. + \hat{m}_j \nabla_k \hat{n}_j - \hat{n}_j \nabla_k \hat{m}_j + \hat{m}_j \nabla_j \hat{n}_k - \hat{n}_j \nabla_j \hat{m}_k \right]. \quad (6)$$

A natural unit for distance is the dipole length $\xi_d = (\hbar/2m_3) \sqrt{\rho_{\parallel}/\lambda_d}$. Similarly, we define units for velocity $v_d \equiv \sqrt{\lambda_d/\rho_{\parallel}}$ and current $j_d \equiv \rho_{\parallel} v_d$. The free energy is minimized under the constraint that $\hat{\mathbf{I}}$ must be parallel to the surface normal $\hat{\mathbf{s}}$ at the walls. We restrict ourself in all following calculations to the large-field limit ($H \gg H_d \equiv \sqrt{\lambda_d/\lambda_h}$), where $\hat{\mathbf{d}}$ is locked to the plane perpendicular to the direction of \mathbf{H} .

A schematic view of the situation we wish to describe is presented in Fig. 1. In our calculations we consider a rectangular area in the xy plane with a length L in the direction of the flow ($-L/2 < x < L/2$) and width D in the y direction ($-D/2 < y < D/2$). We assume translational invariance

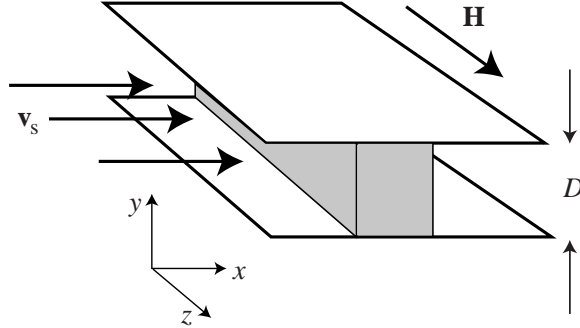


Fig. 1. The parallel-plate geometry used in the calculations. The separation between the plates is D and the superfluid velocity \mathbf{v}_s is in the positive x direction. The orientations of the external magnetic field \mathbf{H} and the soliton wall (grey) are also shown.

in the z direction. The boundary condition at the plate surfaces has the form $\hat{m}_y = \hat{n}_y = 0$. Due to the presence of a large magnetic field $\mathbf{H} \parallel \hat{\mathbf{z}}$, $\hat{d}_z = 0$.

In the numerical calculation the order parameter is defined at $N \times M$ discrete points spaced by Δx and Δy in x and y directions, respectively ($N\Delta x = L$, $M\Delta y = D$). The discretized free energy functional of Eqs. (3)-(5) transforms into a function of the values of $\hat{\mathbf{m}}$, $\hat{\mathbf{n}}$ and $\hat{\mathbf{d}}$ at the lattice points. The minimum of this function is then sought by the following method: first an initial guess for the order-parameter vectors is chosen. Then the texture is changed towards the equilibrium distribution according to

$$\begin{aligned}\Delta \hat{\mathbf{d}} &= \epsilon_d \boldsymbol{\tau}_d \times \hat{\mathbf{d}}, \\ \Delta \hat{\mathbf{m}} &= \epsilon_o \boldsymbol{\tau}_o \times \hat{\mathbf{m}}, \\ \Delta \hat{\mathbf{n}} &= \epsilon_o \boldsymbol{\tau}_o \times \hat{\mathbf{n}},\end{aligned}\tag{7}$$

where the torques acting on the order-parameter vectors are defined as

$$\begin{aligned}\boldsymbol{\tau}_d &\equiv \frac{\delta F}{\delta \hat{\mathbf{d}}} \times \hat{\mathbf{d}}, \\ \boldsymbol{\tau}_o &\equiv \frac{\delta F}{\delta \hat{\mathbf{m}}} \times \hat{\mathbf{m}} + \frac{\delta F}{\delta \hat{\mathbf{n}}} \times \hat{\mathbf{n}},\end{aligned}\tag{8}$$

and the (small) iteration constants ϵ_d and ϵ_o are chosen so as to achieve fast convergence. Also, after each iteration step the vectors are adjusted to have unit length and to satisfy the condition $\hat{\mathbf{m}} \perp \hat{\mathbf{n}}$. The iteration process is

Soliton-limited superflow in $^3\text{He-A}$ between parallel plates

repeated until the minimum of the free energy is reached (signalled by the vanishing of the torques).

We generate the superflow in our model by imposing a fixed difference $\Phi(x = L/2) - \Phi(x = -L/2) \equiv \Delta\Phi$, which will be defined more precisely below. For different values of $\Delta\Phi$, we monitor the average induced supercurrent density

$$j \equiv \langle j_{s,x} \rangle = \frac{1}{D} \int_{-D/2}^{D/2} dy j_{s,x}(x, y), \quad (9)$$

which is independent of x in the converged solution. We study the current-velocity relationship $j(v)$, where $v \equiv (\hbar/2m_3L)\Delta\Phi$ can be interpreted as the velocity of the normal component corresponding to the phase difference $\Delta\Phi$ (Ref. 2). The critical velocity v_c of the flow instability is determined from the condition

$$\left. \frac{\partial j}{\partial v} \right|_{v=v_c} = 0. \quad (10)$$

3. Uniform initial state

Before studying the soliton case, it is necessary to understand the flow response in the absence of the soliton. We begin by considering the simplest order-parameter structure in $^3\text{He-A}$ between parallel plates. For the case of zero velocity, $v = 0$, the free energy is minimized by a uniform texture, where $\hat{\mathbf{l}} \parallel \hat{\mathbf{d}} \parallel \hat{\mathbf{y}}$. This homogeneous configuration is a simultaneous minimum of f_g , f_d , and f_h , and also satisfies the requirement $\hat{\mathbf{l}} \parallel \hat{\mathbf{s}}$ at the boundaries. Next we introduce a flow in the system by a requirement

$$\begin{aligned} \overleftrightarrow{A}(x = L/2, y) &= e^{i\Delta\Phi} \overleftrightarrow{A}(x = -L/2, y) \\ &= e^{2ivm_3L/\hbar} \overleftrightarrow{A}(x = -L/2, y). \end{aligned} \quad (11)$$

In the presence of flow, $\hat{\mathbf{l}}$ tends to turn towards the flow direction because the component of the superfluid-density tensor along $\hat{\mathbf{l}}$, ρ_{\parallel} , is smaller than the perpendicular one, ρ_{\perp} . This would require the formation of an inhomogeneous texture, because at the surfaces of the plates $\hat{\mathbf{l}}$ is rigidly anchored perpendicular to the flow. Therefore, for small enough velocities the uniform texture $\hat{\mathbf{l}} \perp \mathbf{v}_s$ persists as the equilibrium configuration, with $\hat{\mathbf{m}}$ and $\hat{\mathbf{n}}$ turning around constant $\hat{\mathbf{l}}$ to achieve the required phase difference or, equivalently, $\overleftrightarrow{A} = \text{const.} \times \exp(2ivm_3x/\hbar)$.

The transition where $\hat{\mathbf{l}}$ starts to deflect from the plate normal $\hat{\mathbf{y}}$ is known as Fredericksz transition, and v_{Fr} denotes the corresponding velocity. The Fredericksz transition has been studied extensively in the case where it is induced by magnetic field $\mathbf{H} \parallel \hat{\mathbf{y}}$ ¹³. In the present case, it was first calculated

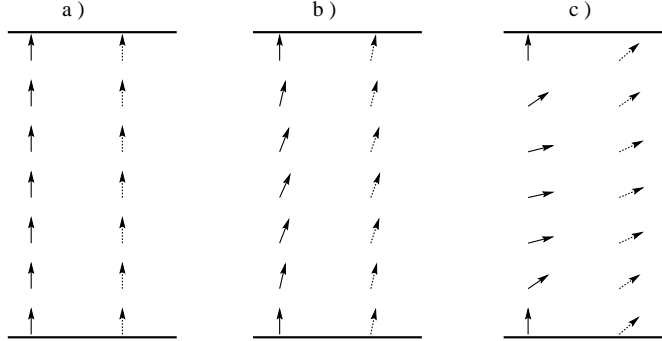


Fig. 2. The variation of $\hat{\mathbf{I}}$ (solid arrows) and $\hat{\mathbf{d}}$ (dashed arrows) for $D = 6\xi_d$, when $v_{\text{Fr}} \approx 0.51v_d$. Both fields are translationally invariant in x direction. The textures are for a) $v < v_{\text{Fr}}$ (homogeneous texture), b) $v = 0.55v_d$, and c) $v = 1.3v_d$.

by deGennes and Rainer³, who neglected the dipole-dipole interaction (3) and obtained

$$v_{\text{Fr}} = \frac{c}{D}, \quad (12)$$

where $c = (\pi\hbar/2m_3)\sqrt{3/4}$. This result holds in the limit $D \ll \xi_d$, but in a wider slab there is additional textural rigidity because $\hat{\mathbf{d}}$ tends to follow $\hat{\mathbf{I}}$. This has been calculated both exactly and by variational ansatz by Fetter⁴. In the limit $D \gg \xi_d$ there is complete dipole-locking and one obtains (12) with $c = (\pi\hbar/2m_3)\sqrt{5/4}$. At intermediate D 's v_{Fr} monotonically interpolates between these limits (see Fig. 9 below).

Typical $\hat{\mathbf{I}}$ and $\hat{\mathbf{d}}$ textures for different values of v are presented in Fig. 2. On increasing the velocity further beyond v_{Fr} , $\hat{\mathbf{I}}$ bends more and more until most of the texture (excluding the vicinity of the surfaces) has aligned itself with the flow direction. Finally, at $v = v_h$, the texture becomes unstable towards helical disturbances that break the translational invariance in the x coordinate⁵, see Fig. 3. We have not made systematic studies of this transition here, but it seems that there is no substantial difference to the corresponding one-dimensional calculation², which corresponds to the limit $D \rightarrow \infty$. The critical velocity increases slightly because of the presence of the lateral walls,

$$v_h(D) \approx v_h(\infty) + \frac{a}{D^2}, \quad (13)$$

where $v_h(\infty) = 1.26v_d$ (Ref. 2) and $a \approx 3v_d\xi_d^2$. Another question is the stability of these helical textures. It has been found in one dimension that the helical textures are unstable towards nucleating vortices in the vicinity

Soliton-limited superflow in $^3\text{He-A}$ between parallel plates

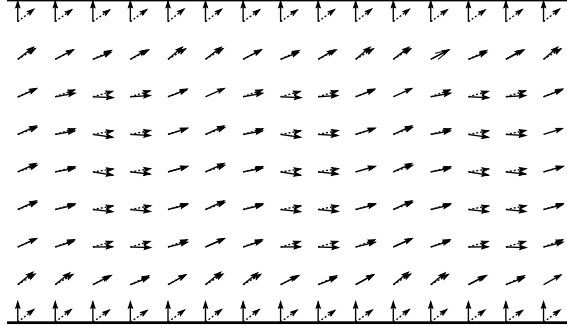


Fig. 3. Helical disturbances of $\hat{\mathbf{l}}$ (solid arrows) and $\hat{\mathbf{d}}$ (dashed arrows) for $D = 8\xi_d$ at $v = 1.3v_d$. A length of $L = 15\xi_d$ in the direction of flow is presented, comprising three wavelengths of the helix.

of T_c ^{6,2}. Whether this is true also in our restricted geometry remains open.

A useful way of expressing the response to an externally applied flow is through the current-velocity diagram $j(v)$. A typical example of such a diagram is presented in Fig. 4. At low velocities the uniform texture with $\hat{\mathbf{l}} \perp \mathbf{v}_s$ can be seen as a linear slope $j = \rho_\perp v$. At the Fredericksz transition part of the $\hat{\mathbf{l}}$ texture starts to deflect towards \mathbf{v}_s , causing a decrease in the slope of j . With increasing velocity the texture tends to align with \mathbf{v}_s and the slope approaches ρ_\parallel .

4. Flow with a soliton

The complicated order-parameter structure of $^3\text{He-A}$ allows for a variety of different topological defects. One variety of these are solitons, i.e. two-dimensional domain-wall-like structures separating two energetically degenerate minima of the dipole-dipole interaction (3). On one side of the soliton $\hat{\mathbf{l}}$ and $\hat{\mathbf{d}}$ are parallel to each other, on the other side antiparallel. In our geometry the soliton has the so-called splay structure, i.e. the magnetic field is in the plane of the soliton, see Fig. 5. Because of the orienting effect of the walls, far away from the soliton a uniform $\hat{\mathbf{l}} = \hat{\mathbf{y}}$ texture is approached, with $\hat{\mathbf{d}} = -\hat{\mathbf{y}}$ on the left side and $\hat{\mathbf{d}} = \hat{\mathbf{y}}$ on the right side of the wall.

The boundary condition (11) we used to generate flow in the uniform case is not consistent with the presence of a soliton. Instead, it is possible to show that the combined operation of translation by L in the flow direction and reflection in the y coordinate is a symmetry operation for the soliton

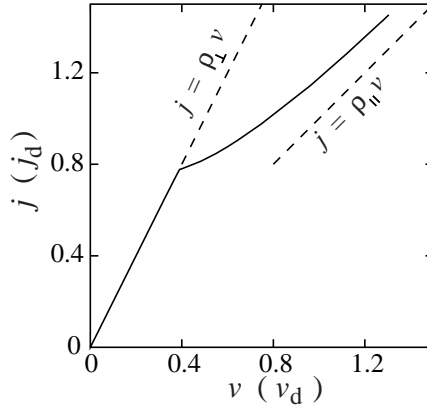


Fig. 4. The current-velocity diagram for $D = 8\xi_d$. The Fredericksz transition shows up as a kink at $v \approx 0.4v_d$ and the curve ends to the onset of helical texture at $v \approx 1.3v_d$. The lines $j = \rho_{\perp}v$ and $j = \rho_{\parallel}v$ are shown as guides to the eye.

texture. Therefore, a flow velocity equal to v can be achieved by requiring

$$\overleftrightarrow{A}(x = L/2, y) = e^{2ivm_3L/\hbar}\sigma_y \overleftrightarrow{A}(x = -L/2, -y)\sigma_y, \quad (14)$$

where σ_y is a diagonal matrix with elements 1, -1, and 1. Otherwise the numerical calculations follow the same procedure as in the case with a uniform initial texture.

In order to understand the response of the soliton wall to an external flow, it is advantageous to first study a simpler case in one dimension x along the flow in the bulk. We consider the range from $x = -L/2$ to $x = L/2$, over which the direction of $\hat{\mathbf{l}}$ is reversed from $\hat{\mathbf{l}} = -\hat{\mathbf{x}}$ to $\hat{\mathbf{l}} = \hat{\mathbf{x}}$, see Fig. 6. In the absence of a magnetic field, it is possible to show that, starting with a texture with zero phase difference over the length L , a texture with a phase difference equal to $\Delta\Phi$ can be formed by simply rotating the initial texture an angle $\Delta\Phi/2$ around $\hat{\mathbf{x}}$. Furthermore, also the final texture carries zero supercurrent. The situation changes if a magnetic field $\mathbf{H} \perp \hat{\mathbf{x}}$ is introduced, because it prevents $\hat{\mathbf{l}}$ from rotating freely through the dipole-dipole interaction. As a result, a texture corresponding to a nonzero supercurrent is formed. When the phase difference exceeds a critical value, the texture undergoes an abrupt rotation through a large angle, again leading to vortex creation somewhere on the sides. Roughly the same scenario takes place also in the two-dimensional parallel-plate geometry, with some modifications. Far away from the soliton plane and at the solid walls the texture is locked to a uniform $\hat{\mathbf{l}} = \hat{\mathbf{y}}$ configuration and cannot rotate when the flow is applied.

Soliton-limited superflow in $^3\text{He-A}$ between parallel plates

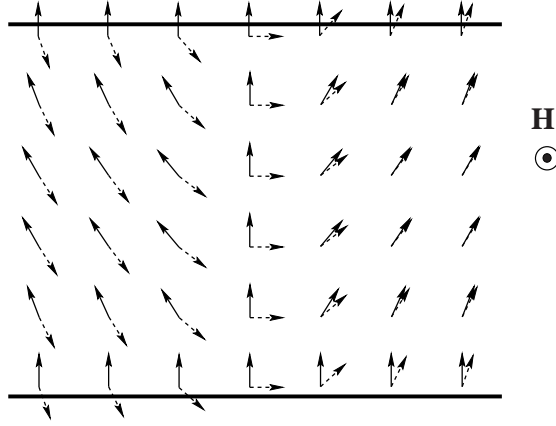


Fig. 5. The variation of $\hat{\mathbf{I}}$ (solid arrows) and $\hat{\mathbf{d}}$ (dashed arrows) in a splay soliton structure for $D = 8\xi_d$ and zero velocity. On the left side $\hat{\mathbf{I}} = -\hat{\mathbf{d}}$ and on the right side $\hat{\mathbf{I}} = \hat{\mathbf{d}}$.

This results in an additional rigidity opposing the rotation of the soliton.

The calculation of the critical velocity for the soliton presents some problems because, due to the breakdown of translational invariance in the x direction, the flow response of the system depends on the length L of our computational region. We define the critical velocity as

$$v_c \equiv \lim_{L \rightarrow \infty} (\hbar/2m_3) \frac{\Delta\Phi_c(L)}{L}, \quad (15)$$

where $\Delta\Phi_c$ corresponds to the phase difference for which the maximum current $j_c(L)$ is achieved. A typical form of the current-velocity diagram at

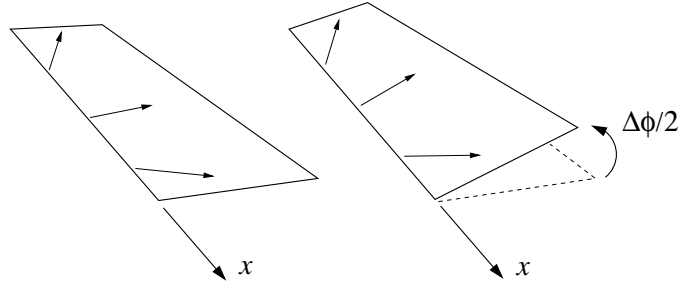


Fig. 6. Flow response of a one-dimensional soliton structure (schematic). A phase difference of $\Delta\Phi$ can be accomplished by rotating texture an angle of $\Delta\Phi/2$ around the flow direction.

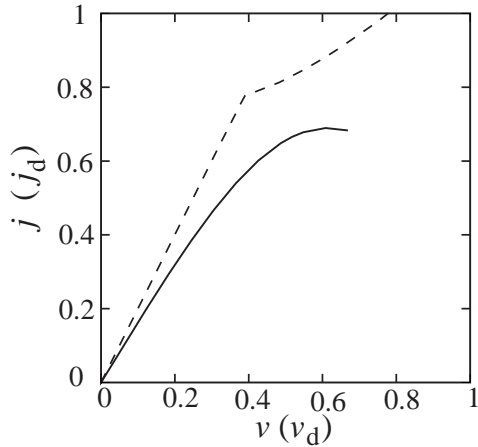


Fig. 7. The current-velocity diagram for a splay soliton texture for $D = L = 8\xi_d$ (solid line). The diagram in the absence of the soliton for a channel of the same width is also shown (dashed line).

finite L is shown in Fig. 7. With increasing L (thus increasing the relative length of the soliton-free region) the current-velocity curve approaches the translationally invariant behavior discussed in the previous chapter. However, it turns out that $v_c(L)$ shows appreciable dependence on L even for $L \gg \xi_d$. On the other hand, the value of the critical current $j_c(L)$ only varies on a much smaller scale (on the order of a few percent). The dependences are presented in Fig. 8. Therefore, in order to avoid lengthy calculations involving a huge number of lattice points, we calculate the critical current using a moderate-sized lattice and read the corresponding velocity v_c from the current-velocity curve without the soliton (such as in Fig. 4).

The critical current j_c for the splay soliton texture is presented in Figs. 9 and 10 as a function of the plate separation D . In Fig. 9 we have plotted the product $j_c D$. We have also included for comparison the numerically calculated $j_{\text{Fr}} D$ and the analytic limits (12) for the Fredericksz transition. In order to have a more accurate look at the limit of large plate separations, we present j_c and $2v_c$ as functions of inverse D in Fig. 10. As long as the critical currents exceed $j_{\text{Fr}} \equiv 2v_{\text{Fr}}$ (i.e. when $D \lesssim 12\xi_d$), the dimensionless critical currents and velocities are simply related through a factor of two: $j_c/j_d = 2v_c/v_d$. However, for large plate separations j exceeds j_{Fr} , and the critical velocity decreases more slowly (see Fig. 4).

From the figures we find that, for intermediate values of D , j_c obeys

Soliton-limited superflow in $^3\text{He-A}$ between parallel plates

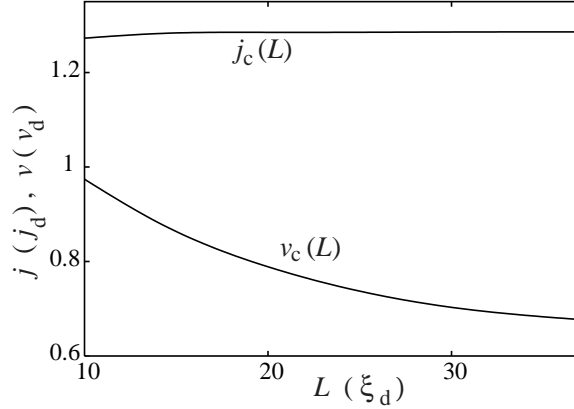


Fig. 8. The critical velocity u_c and current j_c for a splay soliton as functions of L for $D = 4\xi_d$.

reasonably well the relation

$$j_c \approx \frac{a}{D} + b, \quad (16)$$

with $a = 4.5j_d\xi_d$, $b = 0.17j_d$ for $D \lesssim 12\xi_d$, and $a = 5.1j_d\xi_d$, $b = 0.11j_d$ for $D > 12\xi_d$. Fig. 10 suggests that v_c levels off at the limit of large D to $0.15v_d < v_c^{\text{bulk}} < 0.2v_d$, in agreement with our previous result obtained from a one-dimensional treatment of a dipole-unlocked soliton². Note also that $v_c/v_d = j_c/j_d$ in the limit $D \rightarrow \infty$. The main conclusion from the calculations above is that the critical velocity in the presence of a soliton is small and depends essentially on the width D of the channel. The dependence is much stronger than for the helical instability in the absence of the soliton.

The calculation above gives a qualitative explanation for the measured critical velocity of a vortex sheet. The vortex sheet consists of a soliton backbone to which continuous vorticity is added⁹. In a rotating container the sheet has end lines at the side walls of the container. During angular acceleration there is counterflow through the vortex-free end pieces of the sheet, and the sheet can grow only when new vorticity is nucleated there. It is found experimentally that the critical velocity for the growth of the vortex sheet depends essentially on the angular velocity Ω , increasing with increasing Ω ¹⁰. This can now be understood because the width of the vortex-free soliton pieces decreases with increasing Ω , which corresponds to decreasing D in a channel and thus increasing v_c . The channel model is still a rather crude approximation for the end piece of a vortex sheet, but in spite of that it gives the right order of magnitude for the critical current and its dependence on Ω .

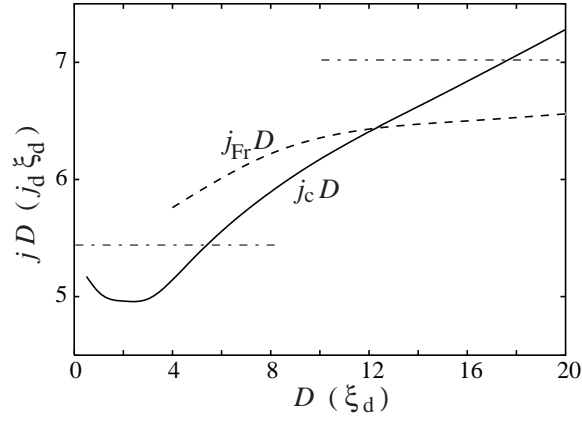


Fig. 9. The critical current j_c times the plate separation D for a splay soliton as a function of D (solid line) Also shown is $j_{Fr}D$ corresponding to the Fredericksz transition of a uniform texture (dashed line), together with analytic results (12) for the limiting cases of dipole-locking (upper dash-dotted line) and for $\hat{\mathbf{d}} = \text{constant}$ (lower dash-dotted line).

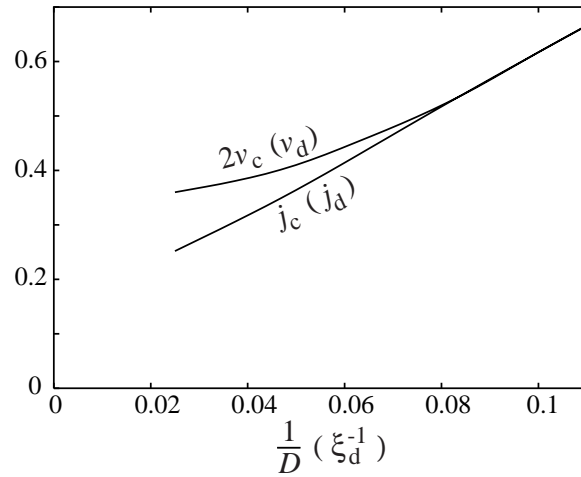


Fig. 10. The critical current j_c and twice the critical velocity $2v_c$ for a splay soliton as a function of $1/D$.

Soliton-limited superflow in $^3\text{He-A}$ between parallel plates

We can argue analogously for the continuous vortex lines. Since we found only weak dependence of the helical instability on the channel width (13), the critical velocity for creating vortex lines should be essentially independent on the rotation velocity. This is what is found experimentally¹⁰.

5. Nuclear magnetic resonance

NMR techniques are effective in obtaining information about the order-parameter distribution in superfluid ^3He . The frequency of the transverse NMR absorption peak is given by^{14,1,9}

$$\omega^2 = \omega_0^2 + R_\perp^2 \omega_\parallel^2, \quad (17)$$

where ω_0 is the Larmor frequency, ω_\parallel the A-phase longitudinal resonance frequency, and R_\perp^2 is determined by solving the eigenvalue problem¹⁴

$$-(2\nabla^2 - \nabla \cdot \hat{\mathbf{I}} \cdot \nabla)\psi + U\psi = (R_\perp^2 - 1)\psi \quad (18)$$

for the transverse fluctuations of $\hat{\mathbf{d}}$ given by the wave function ψ . The potential for the fluctuations is given by

$$U = -\hat{l}_z^2 - (\hat{\mathbf{I}} \times \hat{\mathbf{d}})^2 - 2(\nabla\theta)^2 + (\hat{\mathbf{I}} \cdot \nabla\theta)^2, \quad (19)$$

where $\hat{\mathbf{d}} = \hat{\mathbf{x}} \cos\theta + \hat{\mathbf{y}} \sin\theta$ corresponds to the unperturbed distribution in the presence of a large magnetic field $\mathbf{H} \parallel \hat{\mathbf{z}}$. An approximation for the lowest eigenvalue and the corresponding bound state of fluctuation induced by the rf field can be obtained by the following variational principle:

$$R_\perp^2 - 1 = \min_\psi \frac{\int d^3\mathbf{r} (2|\nabla\psi|^2 - |\hat{\mathbf{I}} \cdot \nabla\psi|^2 + U|\psi|^2)}{\int d^3\mathbf{r} |\psi|^2}. \quad (20)$$

For a uniform state with $\hat{\mathbf{d}} \parallel \hat{\mathbf{I}} \perp \mathbf{H}$, the potential in Eq. (19) vanishes, ψ is constant and the absorption occurs at the bulk frequency given by $R_\perp^2 = 1$. However, dipole-unlocked regions such as the splay soliton define a potential well, and usually give rise to the presence of bound states with frequencies corresponding to $R_\perp^2 < 1$. The effective volume of absorption associated with a given mode in a homogeneous rf field is given by

$$V_{\text{NMR}} = \frac{|\int d^3\mathbf{r} \psi(\mathbf{r}) \exp[-i\theta(\mathbf{r})]|^2}{\int d^3\mathbf{r} |\psi|^2}. \quad (21)$$

In the lowest mode $|\psi|^2$ is expected to accumulate near the minima of the potential energy U , which in our problem occur at the two points where the

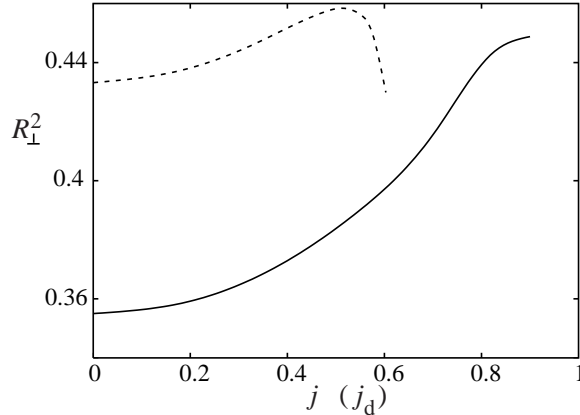


Fig. 11. Transverse NMR frequency shift R_{\perp}^2 as a function of the current j for two different plate separations of $6\xi_d$ (solid line) and $10\xi_d$ (dashed line).

soliton joins the plates. Due to the broken reflection symmetry in $y \rightarrow -y$ ($\hat{\mathbf{s}} \cdot \hat{\mathbf{l}}$ changes sign at the wall, see Fig. 5) two effects arise: the potential wells have different depths, and the directional derivatives $|\hat{\mathbf{l}} \cdot \nabla \psi|^2$ of Eq. (20) give different contributions near the two joining points. As a result, one of the points is singled out as D is increased.

Recent experiments on vortex sheet dynamics have exhibited unexpected behavior¹¹. A possible explanation involves a rotating state that consists of several sheets and multiple contact points with the container. The sheets are joined to the walls by vorticity-free soliton pieces. An important question arising in the explanation is whether these pieces have the same resonance frequencies than the sheet itself. Figure 11 shows R_{\perp}^2 as a function of the flow velocity for two different plate separations. The frequencies we obtained are considerably lower than those associated with bulk splay soliton, calculated e.g. in Ref. 7 for zero velocity as $R_{\perp}^2 = 0.677$. In fact, the frequencies are rather close to the ones expected for a vortex sheet, previously calculated to be $R_{\perp}^2 = 0.46$ – 0.48 , depending on the model⁹.

In addition to the frequency shift associated to a given mode, another important quantity is the relative intensity of the mode. This can be expressed in terms of the effective volume of absorption, V_{NMR} , as defined in Eq. (21). For small values of D , $|\psi|^2$ is distributed almost evenly along the entire soliton, and V_{NMR} grows linearly with increasing D . After D is increased enough, $|\psi|^2$ concentrates at the joining point of the soliton and one of the plates with $y = -D/2$ ($\hat{\mathbf{s}} \cdot \hat{\mathbf{l}} = 1$), resulting in a constant V_{NMR} . Figure 12 shows the effective area of absorption (volume per unit length in z direction) for zero phase difference, $v = 0$. For comparison, we have also

Soliton-limited superflow in $^3\text{He-A}$ between parallel plates

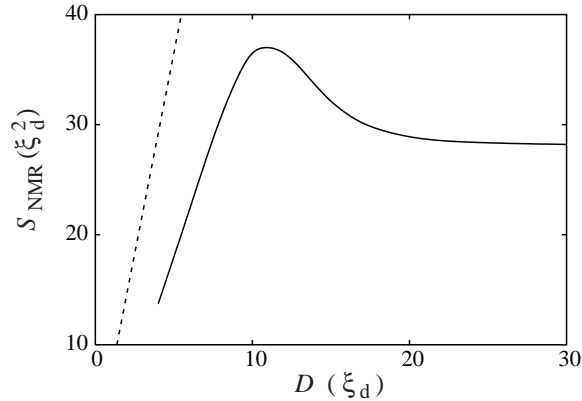


Fig. 12. The effective area of absorption S_{NMR} of the lowest eigenmode as a function of the plate separation D for zero velocity (solid line). Also shown is the area of absorption for a bulk splay soliton of length D (dashed line).

drawn the area of absorption for a bulk splay soliton of length D , calculated to have a absorption thickness of $7.3\xi_d^{15}$. The absorption thickness of a vortex sheet is approximately $6-8\xi_d$ depending on the angular velocity⁹.

6. Conclusions

We have studied the flow stability of superfluid $^3\text{He-A}$ in the vicinity of solid walls by calculating numerically the order-parameter distribution in two spatial dimensions. The emphasis of this work was to study the flow in the presence of a splay composite soliton. We have determined the critical current and velocity for the creation of continuous vortices as functions of the separation between the walls. The results give a qualitative explanation to the experimentally measurable critical velocity for the growth of a vortex sheet. The transverse NMR frequency shift R_{\perp}^2 for the lowest eigenmode of the dipole-unlocked soliton was found to be rather close to that of a vortex sheet.

REFERENCES

1. D. Vollhardt and P. Wölfle, *The Superfluid Phases of Helium 3* (Taylor & Francis, London, 1990).
2. J. Kopu, R. Hänninen, and E. V. Thuneberg, *Phys. Rev. B* **62**, 12374 (2000).
3. P. G. deGennes and D. Rainer, *Phys. Lett.* **46A**, 429 (1974).

J. Kopu and E. V. Thuneberg

4. A. L. Fetter, Phys. Rev. B **14**, 2801 (1976).
5. P. Bhattacharyya, T.-L. Ho, and N. D. Mermin, Phys. Rev. Lett **39**, 1290 (1977).
6. Y. R. Lin-Liu, D. Vollhardt, and K. Maki, Phys. Rev. B **20**, 159 (1979).
7. K. Maki, and P. Kumar, Phys. Rev. B **17**, 1088 (1978).
8. D. Vollhardt and K. Maki, Phys. Rev. B **20**, 963 (1979); **23**, 1489(E) (1981).
9. E. V. Thuneberg, Physica B **210**, 287 (1995).
10. Ü. Parts, V. M. H. Ruutu, J. H. Koivuniemi, M. Krusius, E. V. Thuneberg, and G. E. Volovik, Physica B **210**, 311 (1995).
11. V. B. Eltsov, R. Blaauwgeers, M. Krusius, J. J. Ruohio, and R. Schanen, Physica B **284-288**, 252 (2000).
12. J. M. Karimäki, and E. V. Thuneberg, Phys. Rev. B **60**, 15290 (1999).
13. J. R. Hook, in *Helium Three*, ed. W.P. Halperin and L.P. Pitaevskii (Elsevier, Amsterdam 1990), p. 135.
14. A. L. Fetter, in *Progress in Low Temperature Physics*, Vol. X, ed. D. F. Brewer (North-Holland, Amsterdam, 1986), p. 1.
15. R. Hänninen and E. V. Thuneberg, J. Low Temp. Phys., this issue.